Aerodynamic and Aeroacoustic Analyses of a UAV Propeller with Trailing Edge Serrations

Y. Li (1), Y. Yang (1), Y. Liu (1), Y. Wang (2), B. Huang (2), W. Li (2)

(1) Mechanics and Aerospace Engineering, Southern University of Science and Technology, Shenzhen, China
(2) Institute of Low Speed Aerodynamics, China Aerodynamics Research and Development Center, Mianyang, China

ABSTRACT

Unmanned aerial vehicles (UAVs) can be observed in many applications, e.g. video taking, mapping, construction, delivery, and rescue operation. In some circumstances, the aeroacoustic noise is a big concern and quiet propellers would be more environmentally friendly. Therefore, this research imitates the serrated trailing edge of the owl wings, which are well known for their low noise emissions; the noise reduction and aerodynamic performance of the propeller with trailing edge serrations are analysed. The spectral characteristics, noise reduction and noise directivity of the propeller with serrated trailing edge are measured by microphones in an anechoic wind tunnel. The time-average loading of the propeller with serrated trailing edge and normal propeller are analyzed by a six-component balance. The results show that the noise of the propeller is alleviated, and the noise reduction depends on the Strouhal number and flight conditions. During the forward flight, the maximum noise reduction reaches 12 *dB* when the Strouhal number is around 4. The noise reduction effect is directional, and it is found that the noise reduction on the side of the forward moving blade is significantly larger than the other side. During the hovering condition, the maximum of the noise reduction reaches 7.5 *dB* when the Strouhal number is around 2, and the noise reduction is axisymmetric. The lift and drag of the serrated propeller both decrease by 5% during the forward flight condition, but the lift-to-drag ratio remains the same. The aerodynamic performance of the serrated propeller is not altered during the hovering condition.

1 Background

According to the report of BI intelligence in 2016, it is estimated that global shipments of UAVs will reach more than 20 million by 2020 (BI intelligence, 2016). In the near future, the drone could become a part of our daily life, so its noise emissions may become a concern. Although the noise of small UAVs are relatively low in comparison with helicopters, they are operated at low altitude, and densely populated urban areas. Therefore, this noise is likely to be an important factor that determines its market competitiveness.

$$p'(\vec{x},t)=\frac{1}{c_\infty^2}\frac{\partial}{\partial t}\int_{S_0}\left[\frac{p_\infty V_j n_j}{4\pi r|1-M_r|}\right]_{\tau=\tau^*}dS-\frac{1}{c_\infty^2}\frac{\partial}{\partial x_i}\int_{S_0}\left[\frac{p_{ij}n_j}{4\pi r|1-M_r|}\right]_{\tau=\tau^*}dS+\frac{1}{c_\infty^2}\frac{\partial^2}{\partial x_i\partial x_j}\int_{S_0}\left[\frac{T_{ij}}{4\pi r|1-M_r|}\right]_{\tau=\tau^*}dV \quad (1)$$

As shown in Eq. (1), Ffowcs Williams-Hawkings equation (Ffowcs Williams and Hawkings, 1969), propeller aeroacoustic noise can be mainly divided into three parts: thickness noise, loading noise, and broadband noise. For sufficiently UAVs at a low Mach number, the thickness noise in the FW-H equation can be neglected, because it is relatively small when the Mach number is less than 0.7 (Glegg and Devenport, 2017). Therefore, the propeller noise is mainly determined by loading noise and broadband noise. Limited by task requirements and geometric size, there is little space for the alleviation of steady loading noise. The unsteady loading noise is mainly produced by the pylon-propeller interaction, blade vortex interaction, asymmetrical inflow during forward flight, and inflow turbulence (Frota et al., 1998; Ahmadi, 1985; Sinnige et al., 2017; JanakiRam et al., 2009; Scharpf and Mueller, 1995). It can be noticed that these interactions are due to installation effects, flight mechanisms, and atmospheric conditions of UAVs, and not so much effort can be made here. Therefore, the alleviation of the broadband noise is one of the potential solutions. The broadband noise mechanism of the propeller can refer to two-dimensional airfoils, which is caused by the interactions between turbulence and the blade, including the upstream turbulence interacting with the leading edge (George and Kim, 1976), and the turbulence in the boundary layer interacting with the trailing edge (Brooks et al, 1989). Since the UAV propeller generally utilizes a tractor configuration, the atmosphere turbulence should be smaller than the turbulence in the boundary layer, so it is effective to reduce the trailing-edge broadband noise.

Researches about noise reduction of airfoil with serrated trailing edge are mainly conducted on two dimensional airfoils. Howe (1991) proposed a method for estimating noise reduction of serrated trailing edges, which shows that in the high-frequency range ($fh/U_\infty \gg 1$), the noise reduction reaches $10log_{10}[1+(4h/b)^2]\ dB$, where f is the frequency, $2h$ is the length of the serration, U_∞ is the velocity of the inflow, b is the wave length of the serration. In order to achieve a significant noise reduction, the inclination angle of the serration sides should be less than 45°. For a sinusoidal serrated trailing edge with a low Mach number and a small angle of attack, the noise reduction amplitude for the high frequency region is $10log_{10}[6h/b]\ dB$. Lyu (2016) improved Howe's method by utilizing the prediction model together with flow field data, and found that the noise reduction effect is mainly determined by $k_1 \times 2h$ and $l_z(f)/b$, where k_1 is the streamwise wavenumber of the gust, and $l_z(f)$ is the spanwise correlation length. When these two parameters are larger than 1, the noise will be greatly reduced. The noise is reduced when Strouhal number is less than 30, and the noise reduction achieves the maximum value at Strouhal number 8, which corresponds to the frequency of the inflow instability. Through PIV measurements, it was found that the flow from the pressure side is transported to the suction side at the serration region, so that the large turbulence structures at the trailing edge are destroyed into small turbulence structures, thereby the noise reduces in the low-frequency (Avallone et al., 2016). This observation means that the assumption of the frozen turbulence in the trailing edge region in Howe's theory is not true, which may explain the reason why Howe overpredicted the noise reduction in the high frequency region. León (León et al., 2016) used PIV to measure the flow field near the serrated trailing edge in combination with the TNO-Blake pressure model, found that the attenuated boundary layer and the shear layer of the serration are the main reason for the reduction of surface pressure pulsation.

Besides two dimensional airfoils with serrations, trailing edge serrations are applied on UAV propellers, too. Ning et al. (2017) studied the aerodynamic and aeroacoustic performance of different serration shapes and flight attitudes of the propeller with serrated trailing edges. The results showed that the serrated trailing edge propeller noise was reduced by 0.9-1.6 *dB*. As the ratio of depth to width ratio increases, the noise reduction decreases, and the aerodynamic performance of the serrated trailing edge propeller does not change significantly.

From the literature survey, it is found that trailing edge serrations are effective for the noise reduction of arifoil self-noise, and that lots of criteria are formulated to help design serrations. However, previous research mainly focuses on two dimensional airfoils, while little research is conducted on propellers. Moreover, aerodynamic performance of serrated airfoils and propellers is not well understood, which is significant for UAV manufacturers. Therefore, this research designs a UAV propeller with trailing edge serrations, and investigates its aerodynamic and aeroacoustic performance using force balance and microphone measurements. Time-averaged loading, noise spectrum, noise directivity and noise reduction are analysed for the hovering and forward flight conditions.

2 Experimental setup

This experiment was performed in a low-speed anechoic wind tunnel in China Aerodynamics Research and Development Center. The test section is $0.55\ \mathrm{m} \times 0.4\ \mathrm{m}$, the maximum inflow velocity is $100\ \mathrm{m/s}$, and turbulence level is lower than 0.05%. The background noise level is less than 78 *dBA* at 80 *m/s*, which is measured 2 m away from the wind tunnel centre line, and the cut-off frequency is 100 *Hz*. As shown in Figure 1, the free stream is from the left-hand side to the right hand side. The balance is *ATI Mini* 40 with six-component strain gauges. The ranges of forces and moments in X, Y, and Z directions are $80\ N, 80\ N, 240\ N, 4\ Nm, 4\ Nm, 4\ Nm$, and the measuring resolution of force and moments are $1/50\ N, 1/50\ N, 1/50\ N, 1/2000\ Nm, 1/2000\ Nm, 1/2000\ Nm$. The propeller rotational speed is tuned by the electronic rotational speed controller. Sixteen microphones (*G.R.A.S*. 46AE) are uniformly positioned in a circle with a radius of 0.8 m and 1.37 m below the propeller. All support structures are covered with foams to alleviate the noise from reflections.

The normal propeller and the propeller with serrated trailing edges are shown in Figure 2. The radius of the normal propeller is $0.103\ \mathrm{m}$, and the chord length c at the 3/4 radial position is $0.0163\ \mathrm{m}$. In comparison with the straight two-dimensional airfoil, the trailing edge of the propeller is not a straight line, and the twist angle changes in the radial direction. Therefore, the trailing edge serration design of propeller is more complex than that of two-dimensional airfoils, and the parameters of serration wavelength and height are adjusted accordingly. The average height of the serration $2h$ is 0.1 $c_{3/4R}$, and the width of the serration λ is 0.2 $c_{3/4R}$. The height-to-wave length ratio in our design is lower than other designs for the following reasons (Avallone et al., 2016; León et al., 2016; Suyadi et al., 2017; Ning et al., 2017) for the following reasons. Firstly, the size of the propeller is smaller than the investigated two-dimensional airfoils, and so the serration size is also smaller. The radius of the serration

tip is limited by the CNC (Computerized Numerical Control) machining, and its maximum height can only be achieved AT THE current size. Secondly, although 3D printing may solve the problem of the radius limitation of the serration, the stiffness of these ultra-thin structure and high-aspect-ratio blades cannot meet the design requirements. Thirdly, there was evidence that the prediction model of Howe (1991) may not be correct: it was found that the noise reduction increases for smaller height-width ratio (Ning et al., 2017; Moreau and Doolan, 2013). Moreover, from the experimental results of this study, it is found that our design performs very well in terms of noise reduction, and it is comparable to that of other serration designs.

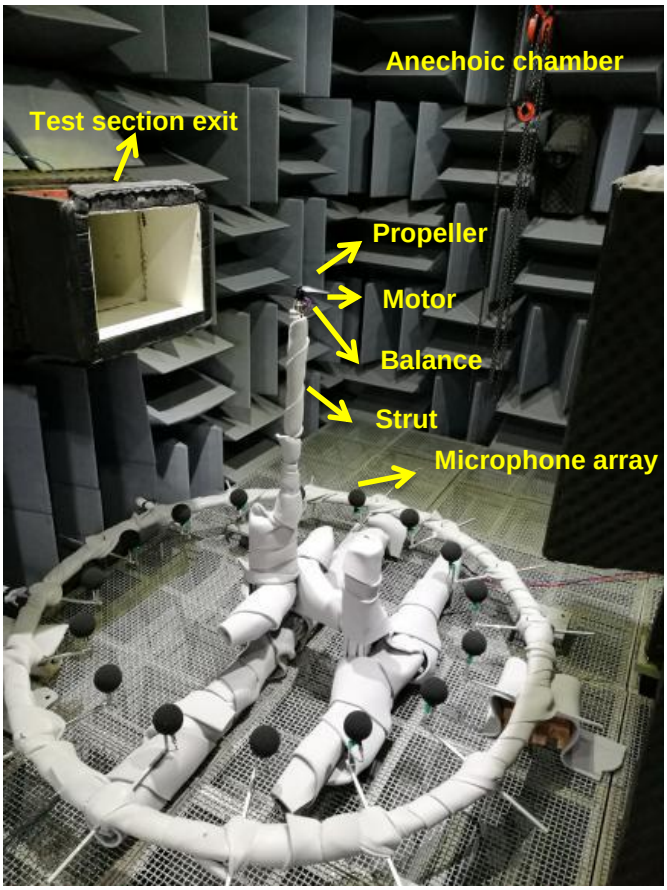

Figure 1: The setup of the wind tunnel test.

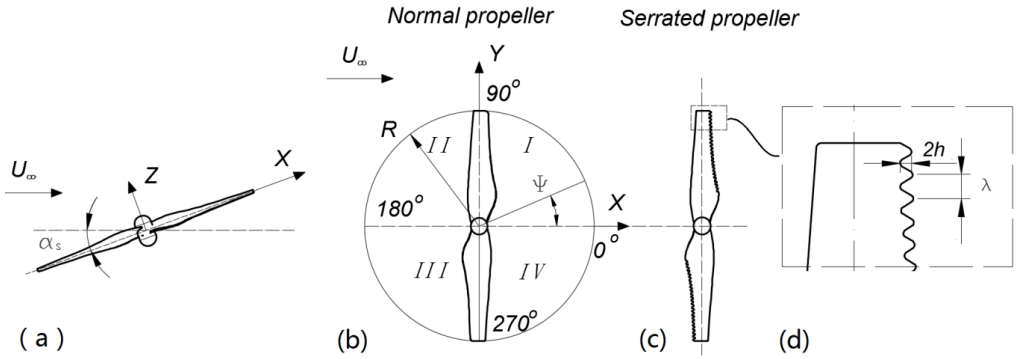

Figure 2: (a) Definitions of the propeller coordinate system and the shaft angle during forward flight. (b) Definition of the phase angle of the blade and quadrants. (c) The planform of the serrated trailing edge propeller. (d) Zoom-in of serrations.

Wind tunnel experiments were carried out at both forward flight and hovering conditions. During the forward flight, the propeller shaft inclined forward by $10°$ and the velocity of the inflow is $10\ m/s$. The flight parameters and the aerodynamic performance of the propeller are defined according to the helicopters, i.e., the advance ratio μ, the lift coefficient C_L, the drag coefficient C_D and efficiency η. These parameters are respectively defined as,

$$\mu = \frac{U_\infty}{2\pi\Omega R} \tag{2}$$

$$C_L = \frac{L}{\rho(\Omega R)^2 A} \tag{3}$$

$$C_D = \frac{D}{\rho(\Omega R)^2 A} \tag{4}$$

$$\eta = \frac{1000*L/g}{\Omega T} \tag{5}$$

U_∞ is the velocity of the free stream, Ω is rotation speed of the propeller, ρ is the air density, A is the area of the propeller disk, T is the tension in the z direction.

During the hovering condition, the flight parameter is characterized by the rotational speed (rpm).The aerodynamic performance is evaluated by the thrust ($T,\ N$), the torque ($Q,\ Nm$), and the efficiency ($\eta,\ g/W$). These parameters during hovering condition are widely used for helicopter, propeller, and UAV manufacturers.

The power spectral density of the noise signal uses ensemble averaging method (Marte, 1970), and the adjacent signal window is 50% overlapped. The resolution of the power spectral density is 0.1 Hz, which is sufficient for resolving the blade passing frequency. The unit of the power spectral density is dB/Hz, and the reference pressure is 20 μPa.

3 Results and discussions

3.1 The noise reduction and aerodynamic performance of the propeller with trailing edge serrations during forward flight

During forward flight, with shaft angle 10°and free stream speed $10\ m/s$, the sound pressure spectrum results are shown in Figure 3. In low-frequency, the sound pressure spectrum features the blade passing frequency (1BPF is shown by the green dotted line in Figure 3) and its harmonics, which are generally considered to be caused by blade steady and unsteady loading noise (Glegg and Devenport, 2017). The steady loading is a result of the propeller rotating at a constant speed, and the unsteady loading is mainly caused by the asymmetrical inflow and the interaction between the tip vortex of the propeller and the blade (JanakiRam et al, 2009; Yang et al., 2018). In the high-frequency range, the spectral characteristics feature broadband noise, which is generally considered to be caused by the interaction between the leading edge of the blade and the inflow turbulence, as well as the interaction between the trailing edge of the blade and the turbulent flow within the blade boundary layer (George and Kim, 1976; Brooks et al., 1989).

The amplitude of the sound pressure spectrum of the serrated trailing edge propeller subtracted by that of the baseline propeller represents the noise reduction, which is shown in Figure 4. The *x*-axis has been nondimensionalized, and the reference length and velocity of the Strouhal number are the chord length and the tangential velocity on the $3/4$ radius of the blade. The maximum frequency of the spectrum is 12800 *Hz*, and the maximum Strouhal number corresponding to different rotational speeds is $St = 3.62{\sim}8.44$. For all tested rotational speeds, the noise reduction is obvious after $St = 0.8$, and the noise reduction reaches the maximum value of 12 *dB* at Strouhal number around 4. The numerical simulation of two-dimensional serrations by Avallone et al. (2018) found that the noise reduction reaches the largest value at $St = 8$. Although the results have the same order of magnitude as the current results, there is still a certain deviation. The main reason for this deviation may be due to the different serration parameters. The serration parameter $2h/\lambda$ in Avallone's work is 2, while the serration parameter of this paper is 0.5. Lyu et al. (2016) found that increasing the parameter $2h/\lambda$l only affects the high-frequency noise, which may be the reason why the most effective Strouhal number of Avallone, is larger than that in the present study.

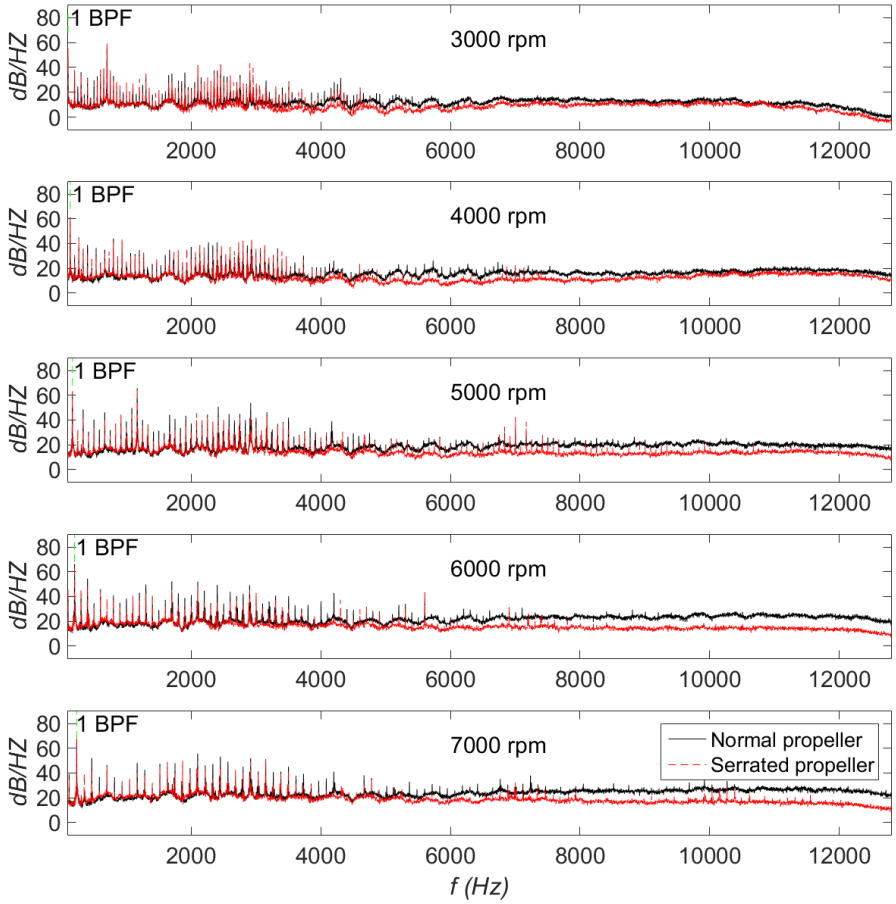

Figure 3: Comparison of the sound pressure spectrum between the baseline propeller and the serrated propeller during forward flight, $U_\infty = 10\,m/s,\ a_S = 10^\circ$. The phase angle of the microphone is $\psi = 135^\circ$.

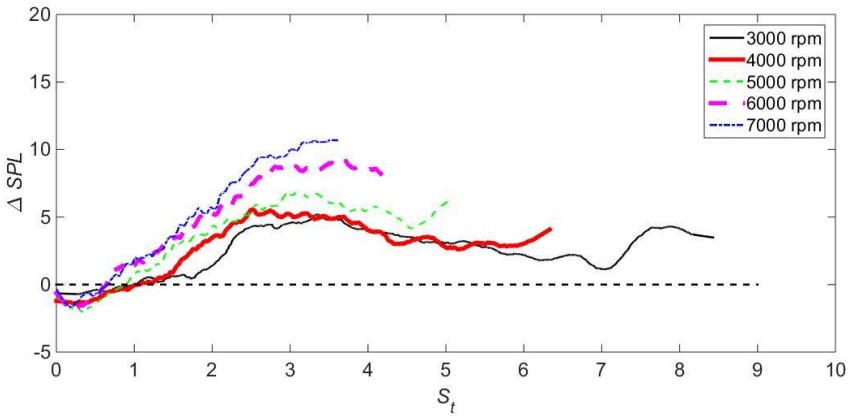

Figure 4: The amplitude of noise reduction between the baseline propeller being subtracted and the serrated propeller during forward flight. The positive value represents noise reduction. $U_\infty = 10\,m/s,\ \ a_S = 10^\circ, \psi = 135^\circ$.

Figure 4 shows that the serrated trailing edge propeller performs well in terms of noise reduction, but this is based on the conclusion of a single microphone. Next, the acoustic data of other locations are analysed to determine whether the noise reduces in other directions. As shown in Figures 4 and 5, the noise reduction of the serrated trailing edge propeller mainly occurs in the high-frequency range, and the noise reduction is larger for higher

rotational speeds. Hence the directivity of noise reduction $\Delta\mathrm{SPL}$ is analysed by integrating the sound pressure level between $6000\ Hz$ and $12800\ Hz$ at $5000\ -7000\ rpm$ for the noise reduction analysis, as shown in Figure. 5. The amplitudes of $\Delta\mathrm{SPL}$ in the first and second quadrants are larger than those in the three and four quadrants, where the definition of the quadrant was shown in Figure. 2(b). As the rotational speed and the Strouhal number increase, the noise reduction increases.

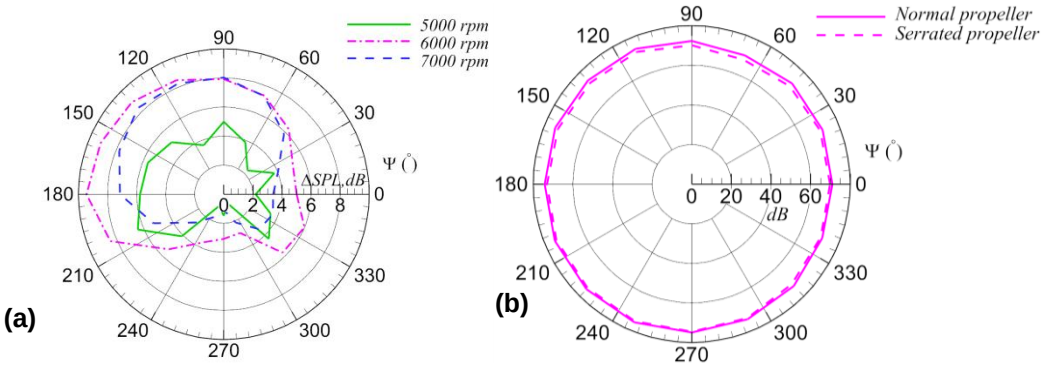

Figure 5: (a) Noise reduction directivity analysed from 6000 Hz to 12800 Hz. (b) The overall sound pressure level directionality of serrated trailing edge propeller noise and the normal propeller noise, $U_\infty = 10\ m/s,\ \ a_S = 10^\circ$.

For the serrated trailing edge propeller, the directivity of the overall sound pressure level is also analysed in comparison with that of the normal propeller. Here the 7000 rpm condition is selected, because the change of the sound pressure is obvious at this condition. It can be seen from Figure 5(b) that the noise of the normal propeller (purple solid line) is almost uniformly distributed in the circumferential direction. The serrations do not affect the directivity of the propeller by comparing the purple solid and dashed curves in Figure 5(b).

The acoustic performance of the serrated propeller is evaluated in the previous analyses, the aerodynamic performance is analysed as follows. As shown in Figure 6(a), the lift coefficient changes with the advance ratio during forward flight. It should be pointed out that the advance ratio μ, as defined in formula (1), decreases when the rotation speed increases. Compared with the baseline propeller, the lift of the serrated trailing edge propeller decreases by 5.34% and 5.13% at μ=0.19 and μ=0.13, respectively. As the lift coefficient decreases, the drag coefficient also decreases accordingly with approximately the same magnitude as shown in Figure 6(b), i.e. 5.32% and 5.79% at μ=0.13 and μ=0.19, respectively.

Since reduction of the lift coefficient is equivalent to that of the drag coefficient, lift-to-drag ratio does not change significantly as shown in Figure 6(c). Compared with the serration design method by extending the chord length at the trailing edge of the baseline propeller (Ning, Wlezien and Hu, 2017), the serration design adopted in this study results in a decrease in lift at the same speed, which should be due to the reduction of the propeller blade area. However, this scheme also found that this method of making the serration by cutting the trailing edge has no effect on the lift-to-drag ratio. Since there is no analysis of the drag and the lift-to-drag ratio in the related research, whether this advantage exists in other design methods have not be verified yet.

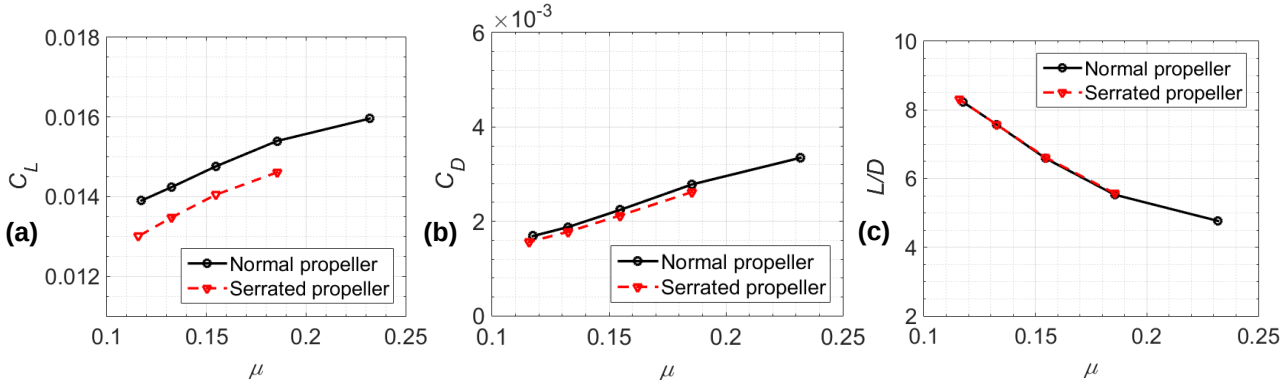

Figure 6: The comparison of the aerodynamic performance between the normal propeller and the serrated trailing edge propeller, $\alpha_S = 10^{\circ}, U_\infty = 10\, m/s$. (a) The thrust coefficient versus the advance ratio. (b) The torque coefficient versus the advance ratio. (c) The lift-to-drag ratio versus the advance ratio.

3.2 The noise reduction and aerodynamic performance of the propeller with trailing edge serrations during the hovering condition

The sound pressure spectra of the propeller during the hovering condition are shown in Figure 7. One observation during hovering condition is that the Sound pressure level at 1 BPF is lower than that at 7 BPF, which implies that the aeroacoustic noise becomes less significant than motor noise. The other observation is that when rpm increases, the noise reduction decreases. The detailed noise reduction plot is shown Figure 8, and the X axis is normalised in the same way as Figure 4. Noise reduction can be observed for almost all Strouhal numbers, and the maximum reduction occurs in the range of $St = 2{\sim}3$.

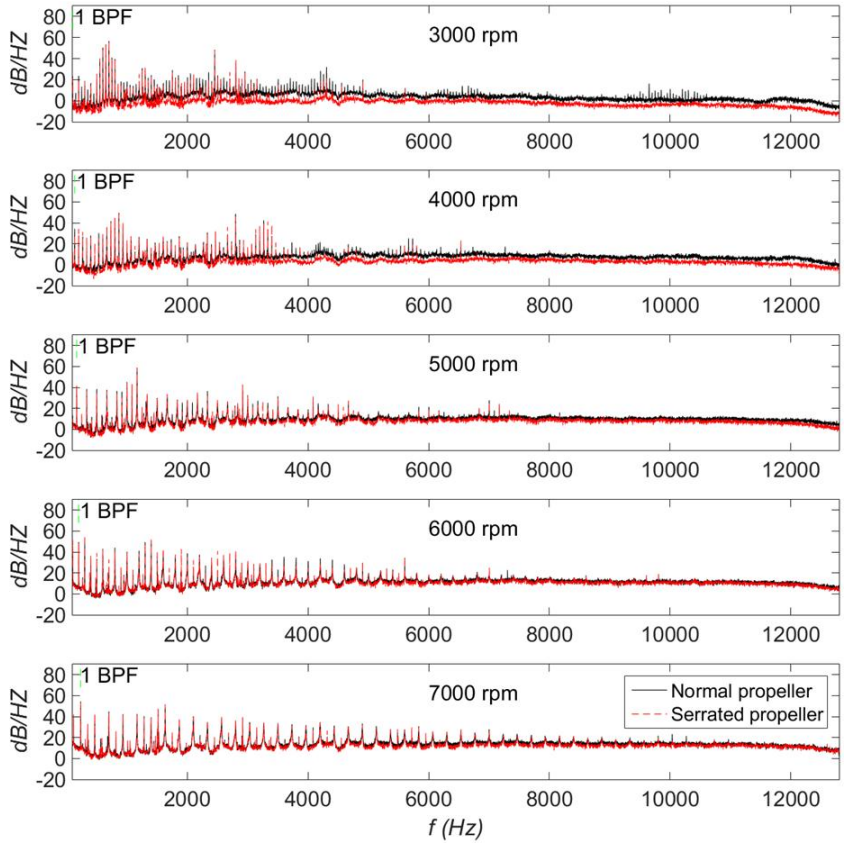

Figure 7: The comparison of the sound pressure frequency spectra of the normal propeller and the serrated propeller during forward flight, $U_\infty = 0\, m/s$, $a_S = 0^{\circ}$, the phase angle of the microphone is $\psi = 135^{\circ}$.

Following the same method for the analysis of the noise reduction directivity during the forward flight condition, the same analysis is performed for the hovering condition. Since there is no asymmetry inflow, the angle of attack, Mach number, and Reynolds number, which are considered to affect the noise reduction effect (Suryadi Martens and Herr, 2017; Lyu, Azarpeyvand and Sinayoko, 2016), are uniform in the circumferential direction. Therefore, the noise reduction is circumferentially uniform.

The aerodynamic performance of the propeller during the hovering condition is shown in Figure 10. It shows that the thrust coefficient, torque coefficient, and efficiency of the serrated propeller have negligible difference from that of the baseline propeller. It implies that the area reduction by cutting serrations on the blade does not affect the forces and moments on the blade, and the lift reduction on the propeller during forward flight could be attributed to other reasons, e.g. the dynamic loading decrease as result of serrations.

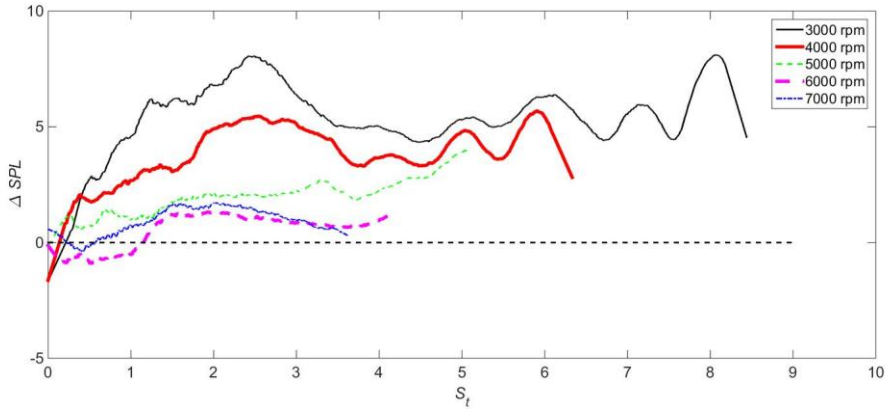

Figure 8: The sound pressure spectra of noise reduction being subtracted by that of the serrated propeller during the hovering condition, and the positive number represent noise reduction, $U_\infty = 0\ m/s,\ \alpha_S = 0^\circ$, the phase angle of the microphone $\psi = 135^\circ$.

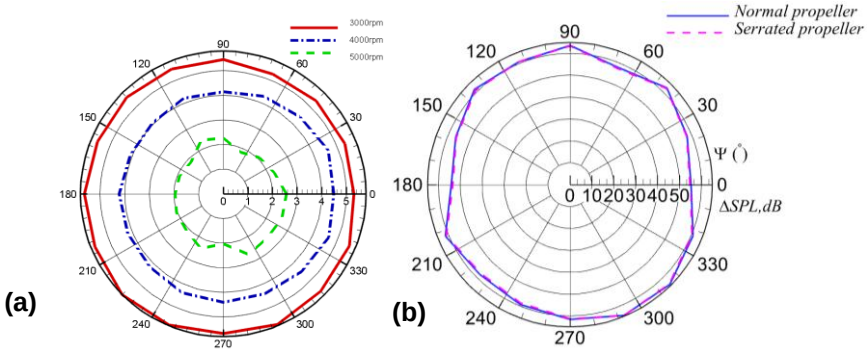

Figure 9: (a) The noise reduction directivity analysed from 6000 Hz to 12800 Hz; (b) The overall sound pressure level directivity of the serrated propeller and the normal propeller

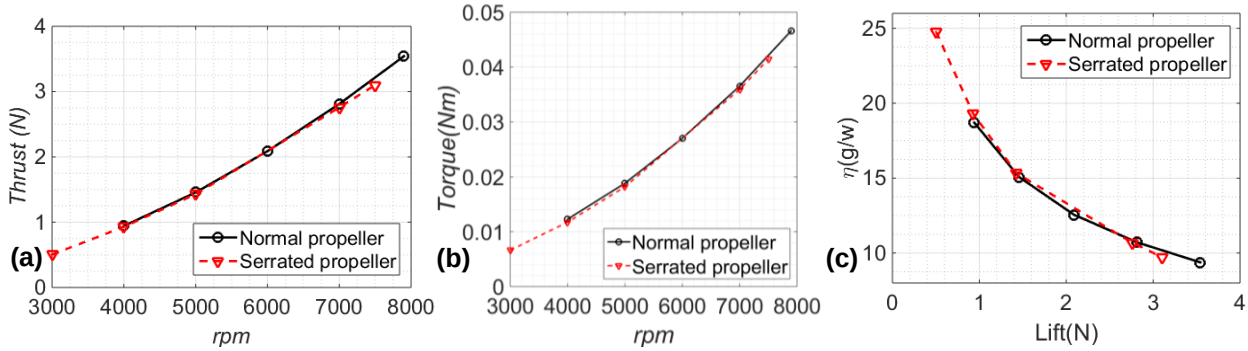

Figure 10: The aerodynamic comparison between the baseline propeller and the serrated propeller, $\alpha_S = 0^\circ, U_\infty = 0\ m/s$. (a) The thrust versus the rotational speed. (b) The torque versus the rotational speed. (c) The efficiency versus the lift.

4 Conclusion

By utilizing microphone and balance measurements, serrated and baseline propellers are analysed in this research. Propeller trailing-edge serrations mainly reduce the broadband noise in the high frequency range. The noise reduction effect is found to depend on several parameters, i.e. Strouhal number, rotation speed, and phase angles.

During the forward flight, the noise reduction in the Strouhal number range of [3,4] performs better than other ranges, and the maximum reduction achieves 12 *dB*. When the rotation speed increases, the noise reduction effect increases accordingly. The noise reduction of the propeller with serrated trailing edge at high rotational speed is larger than that at low rotational speed, and the frequency range with the largest noise reduction magnitude is near St = 4. The noise reduction magnitude in the first and second quadrants is significantly larger than the third and fourth quadrants. This may be related to the rotation direction of the blade relative to the direction of the free stream.

The serrated trailing edge results in a decrease of propeller lift and drag, and the lift-to-drag ratio almost maintains the same. Compared with the serration design method by extending the chord length at the trailing edge of the baseline propeller (Ning, Wlezien and Hu, 2017), a decrease of lift is noticed in this study, which should be due to the reduction of the propeller blade area.

The noise of the serrated propeller during the hovering condition reduces in the high-frequency range as well. The maximum noise reduction is in the range of $St = 2{\sim}3$. The noise reduction at low rotational speed is larger than that at high rotation speed. The noise reduction amplitude has no obvious directivity during the hovering condition. The aerodynamic performance of the propeller has no significant change by comparing the serrated propeller and the baseline propeller.

REFERENCES

BI intelligence. 2016. 'Drones are about to fill the skies within the next 5 years'. http://www.businessinsider.com/the-drones-report-research-use-cases-regulations-and-issues-2016-4-28.

Ffowcs Williams J.E., Hawkings D.L. 1969. 'Sound generation by turbulence and surfaces in arbitrary motion'. *Mathematical and Physical Sciences* 264(1151): 321–342.

Glegg S and Devenport W. 2017. Aeroacoustics of low Mach number flows-Fundamentals, analysis and measurement. 1st ed. USA, Elsevier.

Frota J.M.C., Lempereur P. and Roger M. 1998. 'Computation of the noise of a subsonic propeller at an angle of attack'. *AIAA* 100 (6): 995-998.

Ahmadi A.R. 1985. 'An experimental investigation of blade-vortex interaction at normal incidence'. *AIAA* 23(1): 47-55.

Sinnige T., Ragni D., Malgoezar A.M.N., Eitelberg G., and Veldhuis L. 2017. 'APIAN-INF: an aerodynamic and aeroacoustic investigation of pylon-interaction effects for pusher propellers'. *CEAS Aeronautical Journal* 9(6): 1-16.

JanakiRam R.D., Sim B.W., Kitaplioglu C., and Straub F.K. 2009. 'Blade-vortex interaction noise characteristics of a full-scale active flap rotor'. *American Helicopter Society* 65th Annual Forum, Grapevine.

Scharpf D.F. and Mueller T.J. 1995. 'An experimental investigation of the sources of propeller noise due to the ingestion of turbulence at low speeds'. *Experiments in Fluids* 18(4):277-287.

Ning Z, Wlezien R. and Hu H. 2017. 'An experimental study on small UAV propellers with serrated trailing edges'. *AIAA Aviation*, Denver.

George A.R. and Kim Y.N. 1976. 'High frequency broadband rotor noise'. 3rd *AIAA Aero-Acoustics conference*, Palo Alto.

Brooks T.F., Pope D.S. and Marcolini M.A. 1989. 'Airfoil self-noise and prediction'. NASA Reference Publication 1218.

Howe M. 1991. 'Noise produced by a sawtooth trailing edge'. *The Journal of the Acoustical society of America*. 5: 33-45.

Lyu B., Azarpeyvand M. and Sinayoko S. 2016. 'Prediction of noise from serrated trailing edges'. *Journal of Fluid Mechanics* 793:556-588.

Avallone F., van der Velden W.C.P., Ragni D. and Casalino D. 2018. 'Noise reduction mechanisms of sawtooth and combed-sawtooth trailing-edge serrations'. *Journal of Fluid Mechanics*. 848: 560-591.

Avallone F., Leon C., Probsting S., Lynch K., and Ragni D. 2016. 'Tomographic-PIV investigation of the flow over serrated trailing-edges'.54th *AIAA Aerospace Sciences Meeting*, San Diego.

León C.A., Merino‐Martínez r., Ragni D., Avallone F. and Snellen M. 2016. 'Boundary layer characterization and acoustic measurements of flow-aligned trailing edge serrations'. *Experiments in Fluids* 57: 1-22.

Moreau D.J. and Doolan C.J. 2013. 'Noise-reduction mechanism of a flat-plate serrated trailing edge'. *AIAA Journal* 51(10):556-588.

Welch P.D. 1967. ‘The use of fast Fourier transform for the estimation of power spectra- A method based on time averaging over short. modified periodograms.’ IEEE Trans. *Audio Electroacoust* 15(2): 70-73.

Yang Y., Liu Y., Li Y., Arcondoulis E., Wang Y., Huang B. and Li W. 2018. ‘Aerodynamic and Aeroacoustic characteristics of a multicopter propeller during forward flight’. *AIAA Propulsion and Energy Forum*, Cincinnati.

Suryadi A., Martens S., and Herr, M. 2017. ‘Trailing edge noise reduction technologies for applications in wind energy’. *AIAA Aviation Forum*, Cincinnati.

Marte J.E. 1970. ‘A review of Aerodynamic noise from propellers, rotors, and lift fans’. NASA technical report 32-1462.